

Suppression of Ostwald ripening in active emulsionsDavid Zwicker,^{1,*} Anthony A. Hyman,² and Frank Jülicher^{1,†}¹*Max Planck Institute for the Physics of Complex Systems, 01187 Dresden, Germany*²*Max Planck Institute of Molecular Cell Biology and Genetics, 01307 Dresden, Germany*

(Received 3 February 2015; published 22 July 2015)

Emulsions consisting of droplets immersed in a fluid are typically unstable since they coarsen over time. One important coarsening process is Ostwald ripening, which is driven by the surface tension of the droplets. Stability of emulsions is relevant not only in complex fluids but also in biological cells, which contain liquidlike compartments, e.g., germ granules, Cajal bodies, and centrosomes. Such cellular systems are driven away from equilibrium, e.g., by chemical reactions, and thus can be called active emulsions. In this paper, we study such active emulsions by developing a coarse-grained description of the droplet dynamics, which we analyze for two different chemical reaction schemes. We first consider the simple case of first-order reactions, which leads to stable, monodisperse emulsions in which Ostwald ripening is suppressed within a range of chemical reaction rates. We then consider autocatalytic droplets, which catalyze the production of their own droplet material. Spontaneous nucleation of autocatalytic droplets is strongly suppressed and their emulsions are typically unstable. We show that autocatalytic droplets can be nucleated reliably and their emulsions stabilized by the help of chemically active cores, which catalyze the production of droplet material. In summary, different reaction schemes and catalytic cores can be used to stabilize emulsions and to control their properties.

DOI: [10.1103/PhysRevE.92.012317](https://doi.org/10.1103/PhysRevE.92.012317)

PACS number(s): 82.70.Kj, 87.16.-b, 82.40.-g

I. INTRODUCTION

Emulsions are mixtures of immiscible liquids, in which droplet formation is typical. Such systems are important in many areas such as pharmaceuticals, foods, and cosmetics, where properties like the droplet size distribution and its stability must be controlled [1]. Besides these technological applications, droplet formation is also important in biological systems. For instance, droplets form compartments in the intracellular fluid [2–6]. Additionally, liquidlike lipid domains are known to structure the cell membrane [7]. One key aspect of biological systems is that they are active, i.e., they are driven away from equilibrium. Recently, we have shown that nonequilibrium chemical reactions could control the formation of centrosomes [5], which are one example for liquidlike substructures in cells. In particular, we suggested that two centrosomes are nucleated by catalytically active cores and grow by an autocatalytic reaction. We also demonstrated that the catalytic cores help to suppress Ostwald ripening and that two coexisting centrosomes can be stable [5]. This raises the questions by what mechanisms chemical reactions could suppress Ostwald ripening in emulsions and under what conditions chemically active emulsions could be stable.

Stabilizing emulsions over long times is a major challenge [1]. This is because emulsions typically coarsen, i.e., large droplets grow and small droplets disappear, which is energetically favorable. There are two different processes that lead to coarsening: droplet coalescence, which is driven by the Brownian motion of droplets, and Ostwald ripening, which is driven by diffusive fluxes between droplets [8,9]. Both these processes have to be suppressed to stabilize emulsions. Droplet coalescence can be suppressed in a number of ways, e.g.,

by utilizing surfactants [10,11] or by simply immobilizing the droplets [12,13]. In contrast, the diffusive flux leading to Ostwald ripening is more difficult to suppress. It can be prevented by trapping particles inside droplets that are insoluble in the surrounding fluid [14–16].

Droplet coarsening due to Ostwald ripening can be suppressed by continuous shearing of a system [17,18]. Shear flows break up larger droplets and thus counteract droplet coarsening. The droplets are in this case typically nonspherical [19,20]. This raises the question of whether other nonequilibrium conditions could also have an effect on droplet coarsening and the stabilization of emulsions. In fact, chemical reactions influence the phase separation kinetics of mixtures, leading to pattern formation and introducing characteristic length scales [21–24]. Furthermore, more complex reaction schemes such as autocatalytic reactions have been shown to add interesting effects, including patterns with multiple length scales [25,26]. Interestingly, a simple case of first-order reactions in an infinite system is formally related to a phase-separating system with long-ranged repulsive interactions [22]. Therefore, phase separation with long-range repulsion is an interesting precedent for suppression of Ostwald ripening [27–31], which by formal analogy provides useful information for the study of droplets with chemical reactions.

In this paper, we study the role of chemical reactions on droplet dynamics in systems of coexisting liquid phases. We introduce a general framework to study such active emulsions both in finite and infinite systems. We use it to show that Ostwald ripening can be suppressed and emulsions are typically monodisperse when first-order chemical reactions are considered. We discuss the typical droplet size and the characteristic rates of the droplet dynamics and we use these results to identify the regions in parameter space where active emulsions are stable. We also test our results by comparing them to numerical solutions. In addition to the simple case of first-order kinetics, we also investigate droplets with autocatalytic reactions, which can describe, for example, the

*Present address: School of Engineering and Applied Sciences, Harvard University, Cambridge, MA 02138, USA.

†Corresponding author: julicher@pks.mpg.de

dynamics of centrosomes [5]. These droplets catalyze their own growth and are best discussed in a ternary fluid. One important property of autocatalytic droplets is that they are hard to nucleate and tend to be unstable. We discuss nucleation of autocatalytic droplets by active cores that catalyze the production of droplet material. These active cores can also suppress Ostwald ripening and stabilize autocatalytic droplets.

The paper is organized as follows. In Sec. II, we introduce a continuum theory of phase-separating fluids with chemical reactions and obtain a coarse-grained description of active emulsions. In Sec. III, we study the simple case of first-order kinetics in a binary fluid. In Sec. IV, we consider autocatalytic droplets in a ternary fluid as an example for a more complex reaction scheme. The results are discussed in Sec. V. Throughout the paper, we compare our results to the classical case of passive droplets without chemical reactions.

II. THEORETICAL DESCRIPTION OF ACTIVE EMULSIONS

We study droplets of a liquid phase that coexists with the surrounding fluid. We consider chemical reactions that can convert soluble components A in the fluid into droplet material B that phase separates from the fluid. We first discuss a continuum theory and then derive dynamic equations for droplet sizes in the emulsion.

A. Continuum theory of ternary fluids

We consider a ternary fluid consisting of soluble building blocks A , droplet material B , and components of the background fluid C , which do not participate in the chemical reactions. Volume fractions of components A and B are denoted $\phi^A(\mathbf{r}, t)$ and $\phi^B(\mathbf{r}, t)$, respectively; the volume fraction ϕ^C obeys $\phi^C = 1 - \phi^A - \phi^B$. For an incompressible, isothermal fluid with constant molecular volumes, the free energy density f depends on the two volume fractions ϕ^A and ϕ^B . For simplicity, we use the form

$$f(\phi^A, \phi^B) = \frac{a}{2}(\phi^A)^2 + \frac{b}{2\psi^2}(\phi^B)^2(\psi - \phi^B)^2, \quad (1)$$

where the positive parameters a and b characterize molecular interactions and entropic contributions. The double-well potential described by the second term accounts for the separation into two phases, a C -rich phase with $\phi^B = 0$ and a B -rich phase with $\phi^B = \psi$, while A distributes freely between both phases [32]. Here, we consider the strong segregation limit, where the volume fraction ϕ^B can vanish in one of the phases.

We are interested in heterogeneous systems where many B droplets coexist with the C phase, see Fig. 1(a). Such systems are globally out of equilibrium but in a local equilibrium approximation the free energy density can be defined in each local volume element. The state of the system is then characterized by the total free energy

$$F = \int \left[f(\phi^A, \phi^B) + \frac{\tilde{\kappa}}{2}(\nabla\phi^A)^2 + \frac{\kappa}{2}(\nabla\phi^B)^2 \right] d^3r, \quad (2)$$

where the integral is over the system volume. Here the terms proportional to $\tilde{\kappa}$ and κ penalize strong gradients, which in particular occur in the interface region between phases

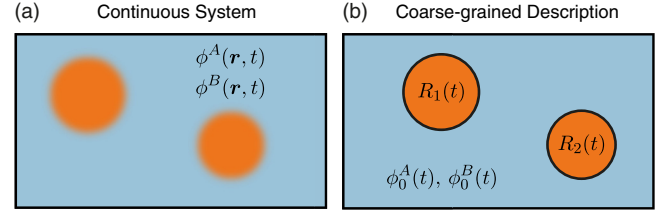


FIG. 1. (Color online) Schematic representations of emulsions with droplets of enriched B components (dark orange) in a background of A components (light blue). (a) Full spatiotemporal description of the volume fractions ϕ^A and ϕ^B including diffuse interfaces. (b) Simplified description in terms of the droplet radii R_i and the average volume fractions ϕ_0^A and ϕ_0^B in the background fluid.

[33]. The width of such interfaces can be discussed by considering a flat interface between two phases with volume fractions $\phi^B = 0$ and $\phi^B = \psi$ far from the interface. In this case, F is minimized by $\phi^B(x) = \frac{1}{2}\psi[1 + \tanh(x/w)]$, where $w = 2(\kappa/b)^{1/2}$ is the interface width and x a coordinate normal to the interface [33]. The free energy associated with the interface per unit area yields the surface tension $\gamma = \frac{1}{6}\psi^2(b\kappa)^{1/2}$ [32].

These expressions for w and γ also hold in the case of curved interfaces, as long as the radius of curvature is large compared to w . Because the surface tension is positive, the free energy F is minimized by droplet configurations with minimal interface area [34]. In emulsions, larger droplets, which have a smaller surface-to-volume ratio, are thus energetically favored over multiple smaller droplets with the same volume. This minimization of the interfacial area drives Ostwald ripening in passive fluids [8].

The dynamics of the concentration fields are described by the equations [22,23]

$$\partial_t \phi^A = m_A \nabla^2 \frac{\delta F[\phi^A, \phi^B]}{\delta \phi^A} - s(\phi^A, \phi^B), \quad (3a)$$

$$\partial_t \phi^B = m_B \nabla^2 \frac{\delta F[\phi^A, \phi^B]}{\delta \phi^B} + s(\phi^A, \phi^B), \quad (3b)$$

where the first terms describe particle-number-conserving diffusive movements and chemical reactions are introduced by a source and sink term s . Here m_A and m_B denote mobilities of the components and we neglect hydrodynamic effects for simplicity [32].

B. Chemical reaction schemes

We discuss chemical reactions in which soluble building blocks A are transformed into droplet material B , while the components C are not changed by the chemical reactions. The reaction flux introduces a source s in Eq. (3). We consider the form

$$s = k_f \phi^A - k_b \phi^B + k \phi^A \phi^B + \phi^A \sum_{i=1}^N Q_i \delta(\mathbf{r} - \mathbf{r}_i). \quad (4)$$

Here the first-order reactions $A \rightarrow B$ and $A \leftarrow B$ have the rates k_f and k_b , respectively, and the rate k describes the autocatalytic reaction $A + B \rightarrow 2B$. We also introduce catalytically active cores that locally catalyze the reaction

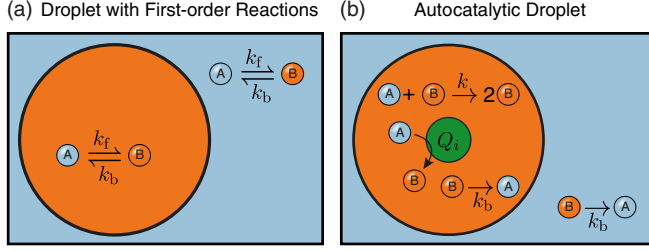


FIG. 2. (Color online) Chemical reaction schemes of building blocks A (light blue) and droplet material B (medium orange) considered in this paper. (a) First-order reactions. (b) Autocatalytic droplets where B is produced by the reaction $A + B \rightarrow 2B$ and at the catalytic cores (dark green), such that the production is effectively restricted to inside the droplets. Droplet material B is converted back to A by a simple first-order reaction.

$A \rightarrow B$ and that therefore can nucleate droplets. The catalytic activity of the core numbered i at position \mathbf{r}_i is denoted by Q_i , see Fig. 2.

Equations (3) and (4) are completed by no-flux boundary conditions. For the reaction schemes considered here, the total amount of components A and B is conserved, and thus the total volume fraction $\bar{\phi} = \bar{\phi}^A + \bar{\phi}^B$ is time independent where

$$\bar{\phi}^i = \frac{1}{V_s} \int \phi^i d^3r \quad (5)$$

denotes the average volume fraction of component i in the system, for $i = A, B$. Here the integral is over the entire system of volume V_s . Note that when chemical reactions are absent ($s = 0$), components A and B are not converted into each other and the volume fractions ϕ^A and ϕ^B are conserved separately.

When expressing the reaction rates by Eq. (4), we have not imposed a detailed balance condition for $A \rightleftharpoons B$ [35,36]. This implicit breaking of detailed balance is important in the following as it gives rise to the rich physics of active droplets developed here. This is motivated in particular by biological systems, where detailed balance is broken, e.g., by the supply of a chemical fuel such as adenosine triphosphate [37]. That breaking of detailed balance is important for droplets to be stable can be seen as follows. If the chemical reactions would obey detailed balance, the system could relax to a thermodynamic equilibrium state for which the free energy F is minimal. Since the components A and B can be converted into each other, there are no separate constraints on the numbers of A and B molecules. As a consequence, the volume fractions ϕ^A and ϕ^B could relax to the values at which the free energy density f has a minimum for a given total molecule number. This is in general a homogeneous, mixed state without droplets [35]. A state with droplets could always lower its free energy by shrinking the droplets and thereby removing the free energy associated with surface tension. Therefore, in the following we only consider nonequilibrium situations in which detailed balance of the chemical reactions is broken and droplets can be stable.

C. Dynamics of active emulsions

We first consider the dynamics of an individual droplet with radius R . Two different volume fractions ϕ_-^B and ϕ_+^B coexist

inside and outside of the interface, respectively. The conditions of coexistence are governed by local thermodynamic equilibrium at the interface. This local equilibrium condition holds if chemical reactions rates are sufficiently small. The chemical potentials of the droplet material are equal on both sides of the interface and the pressure difference between the inside and outside of the droplet is given by the Laplace pressure $2\gamma R^{-1}$. The equilibrium volume fractions inside and outside of the interface can be determined from these thermodynamic principles, see Appendix A. They are given by

$$\phi_-^B \approx \psi \quad \text{and} \quad \phi_+^B(R) \approx \frac{\gamma\beta}{R}, \quad (6)$$

for small surface tension, $\gamma \ll \psi R\beta^{-1}$. Here the coefficient $\beta = 2/(b\psi)$ describes the effect of Laplace pressure on the volume fraction at the interface. Note that $\gamma\beta$ defines a length scale, which is related to the interface width by $\gamma\beta = w\psi/6$. Additionally, the coexistence at the interface requires that ϕ^A is continuous across the interface, see Appendix A, while $\phi^C = 1 - \phi^A - \phi^B$ exhibits a discontinuity at the interface.

The volume fractions ϕ^A and ϕ^B vary on length scales that are large compared to the interface width w . We thus approximate the Eqs. (3) by reaction-diffusion equations inside and outside the droplet,

$$\partial_t \phi^A = D_A \nabla^2 \phi^A - s(\phi^A, \phi^B), \quad (7a)$$

$$\partial_t \phi^B = D_B \nabla^2 \phi^B + s(\phi^A, \phi^B), \quad (7b)$$

where $D_A = m_A a$ and $D_B = m_B b$ are diffusivities.

The volume fraction profile ϕ^B within a spherical droplet can be discussed using Eqs. (7). The radial profile $\phi^B(r)$ varies on a characteristic length scale $l = [D_B/(k_f + k_b)]^{1/2}$, where we have used Eqs. (7) without the contributions of the autocatalytic reaction, because it does not lead to strong gradients inside the droplet, see Appendix B. In the following, we focus on the simple case where l is large compared to the droplet radius R , i.e., chemical reactions rates are small compared to $D_B R^{-2}$. In this case droplets are homogeneous and we thus have $\phi^B \simeq \psi$ inside the droplet, set by the equilibrium solution at the interface, see Eq. (6).

The volume fraction ϕ^B outside of droplets can also be discussed for a spherical droplet. Here $\phi^B(r)$ exhibits the same characteristic length scale l given above, since ϕ^B is typically small and the contribution of the autocatalytic reaction is thus negligible. The total volume flux of component B passing a spherical shell at distance r is given by $J(r) = -4\pi r^2 D_B \partial_r \phi^B(r)$. In particular, we are interested in the flux $J = \lim_{\epsilon \rightarrow 0} J(R + \epsilon)$ of droplet material outside of the interface. In a steady state, where $\phi^B(r)$ approaches the volume fraction ϕ_0^B at large r , we obtain

$$J = 4\pi R D_B (1 + Rl^{-1}) [\phi_+^B(R) - \phi_0^B], \quad (8)$$

see Appendix C. Note that the term Rl^{-1} can be neglected for small droplets or small reaction rates ($R \ll l$). In this case and for $D_A \approx D_B$, the volume fraction $\phi^A(\mathbf{r})$ will be approximately homogeneous throughout the system and we thus approximate $\phi^A = \phi_0^A$. These arguments also show that droplets are inhomogeneous if chemical reactions are fast

($R \gg l$). However, as shown below these droplets are typically unstable.

We can now discuss the dynamics of N droplets $i = 1, \dots, N$ of radii R_i that are sufficiently far from each other that they do not interact directly. Droplet growth is driven by the addition of B components to droplets. Changes in the droplet volume $V_i = \frac{4\pi}{3}R_i^3$ can thus be related to the flux J_i and the chemical reactions inside the droplet. Combining these two effects, the volume growth rate can be expressed as

$$\psi \frac{dV_i}{dt} = (k_f \phi_0^A - k_b \psi + k \phi_0^A \psi) V_i + Q_i \phi_0^A - J_i, \quad (9)$$

where we again consider small droplets or small reaction rates ($0 < R_i \ll l$). Here the term proportional to V_i accounts for the reactions in the bulk of the droplet and the term proportional to Q_i describes the activity of a catalytic core inside the droplet. The dynamics of the average volume fraction of B in the background fluid is given by

$$\frac{d\phi_0^B}{dt} \approx k_f \phi_0^A - k_b \phi_0^B + k \phi_0^A \phi_0^B + \frac{1}{V_s - V_{\text{tot}}} \sum_{i=1}^N J_i, \quad (10)$$

where

$$J_i = 4\pi R_i D_B (1 + R_i l^{-1}) [\phi_+^B(R_i) - \phi_0^B], \quad (11)$$

and $V_{\text{tot}} = \sum_i V_i$ is the total volume of all droplets. Here we have neglected spatial correlations between ϕ^A and ϕ^B in the autocatalytic term. Note that the average volume fraction ϕ_0^A of building blocks reads

$$\phi_0^A = \bar{\phi} - \frac{V_s - V_{\text{tot}}}{V_s} \phi_0^B - \frac{V_{\text{tot}}}{V_s} \psi, \quad (12)$$

which results from the mass conservation given in Eq. (5).

We thus arrive at an effective description of dynamic droplets in the presence of chemical reactions. The state of the system is characterized by the droplet volumes V_i and the volume fraction ϕ_0^B in the background fluid. Their dynamics are governed by Eqs. (10)–(12). The case of conventional emulsions without chemical reactions is found in the limit $k_f = 0, k_b = 0, k = 0$, and $Q = 0$. This case, which we call the passive case, has been well characterized and exhibits Ostwald ripening [38,39]. In the next two sections, we focus on the effects of first-order and autocatalytic reactions on the droplet behavior and compare these active cases to the passive one.

III. DROPLETS WITH FIRST-ORDER REACTIONS

Droplets under the influence of first-order reactions [$k_f > 0, k_b > 0, k = 0, Q_i = 0$, see Fig. 2(a)] can be most easily discussed in the case of a binary fluid. Therefore, we remove component C for this system, such that $\phi^A = 1 - \phi^B$. That is, we consider a system where components A and B undergo chemical reactions and phase separate from each other. The associated free energy density is $f(\phi^B) = \frac{b}{2}(\phi^B)^2(\psi - \phi^B)^2$. The dynamics of the system is of the form of Eq. (3b), with $\phi^A = 1 - \phi^B$ and s given in Eq. (4).

An emulsion of these droplets can be described by the droplet radii R_i and the average volume fraction ϕ_0^B in the background fluid. For the binary fluid, we can write the droplet

growth rate given by Eq. (9) as

$$\frac{dR_i}{dt} = D_B \left(\frac{\phi_0^B}{R_i} - \frac{\gamma\beta}{R_i^2} \right) - \frac{k_b R_i}{3}, \quad (13)$$

where we consider small droplets ($0 < R_i \ll l$) that form by strong phase separation, such that the volume fraction of A components in the droplet is negligible ($\psi = 1$). The volume fraction ϕ_0^B changes with a rate

$$\frac{d\phi_0^B}{dt} = k_f(1 - \phi_0^B) - k_b \phi_0^B + \frac{1}{V_s} \sum_{i=1}^N J_i \quad (14)$$

if the total droplet volume is small compared to the system volume, $V_{\text{tot}} \ll V_s$, see Eq. (10). In the following, we analyze these equations for one, two, and more droplets.

A. Dynamics of a single droplet

1. Large system size

We first investigate a single droplet in the thermodynamic limit of a large system. Because of the large system size, the single droplet does not influence the volume fraction ϕ_0^B in the background fluid and ϕ_0^B is thus constant. The growth dynamics of the single droplet can then be discussed by considering Eq. (13) only.

In a passive system where chemical reactions are absent ($k_f = k_b = 0$), the average volume fraction of component B is conserved and ϕ_0^B is thus set by the initial condition. In this case, a droplet grows indefinitely if it is larger than a critical size R_{crit} , see the orange line in Fig. 3(a). This critical radius corresponds to the single steady state of Eq. (13), where $R = R_{\text{crit}}$ with $R_{\text{crit}} = \gamma\beta/\phi_0^B$. This steady state is unstable, such that droplets with a radius larger than R_{crit} grow, while smaller droplets shrink and disappear.

In the case of first-order reactions ($k_f > 0, k_b > 0$), the average fraction ϕ_0^B in the background fluid is set by the balance of the chemical reactions. Thus, we have

$$\phi_0^B = k_f/(k_f + k_b), \quad (15)$$

which is the steady-state solution of Eq. (14) for large V_s . In this case, there exists a critical radius that is similar to the passive case discussed above, see Fig. 3(a). In particular, the associated steady state of Eq. (13) at $R = R_{\text{crit}}$ is given by $R_{\text{crit}} \approx \gamma\beta/\phi_0^B$ for small reaction rates. However, in contrast to the passive case, large droplets shrink in the presence of chemical reactions according to Eq. (13). Consequently, there exists a stable steady state with a droplet radius \bar{R} larger than R_{crit} , see Fig. 3(a). For large systems, the stable radius of a single droplet reads

$$\bar{R} \approx \left[\frac{3D_B k_f}{(k_f + k_b)k_b} \right]^{\frac{1}{2}}, \quad (16)$$

which follows from Eq. (13) in steady state for small surface tension, $\gamma \ll \bar{R}\phi_0^B/\beta$. The radius \bar{R} diverges for vanishing chemical reactions, such that a droplet in a passive system grows indefinitely, as discussed above. Conversely, \bar{R} is finite in the presence of chemical reactions and faster reaction rates generally lead to smaller droplets, see Fig. 3(b). Importantly, Eq. (16) is only valid if the droplet radius \bar{R} is larger than the

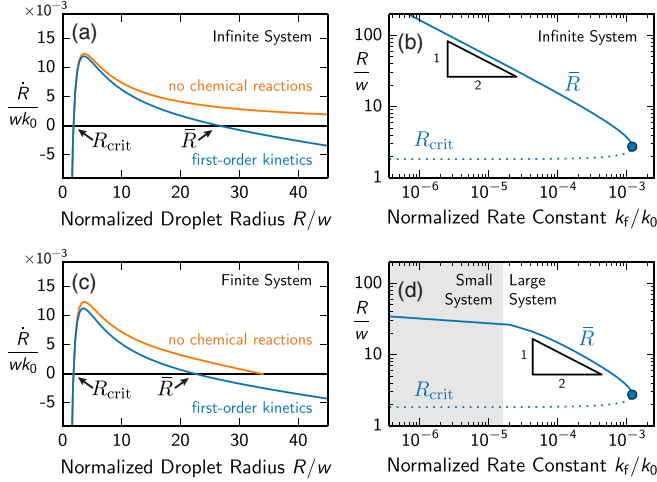


FIG. 3. (Color online) Behavior of a single droplet with first-order reactions. (a) Growth rate $\dot{R} = dR/dt$ given in Eq. (13) as a function of the droplet radius R in an infinite system. The passive system (light orange, $k_f = k_b = 0$, $\bar{\phi}^B = 1/11$) is compared to droplets with first-order kinetics (dark blue, $k_f/k_0 = 3.6 \times 10^{-5}$, $k_b/k_0 = 3.6 \times 10^{-4}$). The critical radius R_{crit} and the stable radius \bar{R} are indicated. (b) Bifurcation diagram of the droplet radius as a function of the rate constant k_f with $k_b = 10k_f$. \bar{R} (solid line) and R_{crit} (dotted line) were determined by solving Eq. (13) numerically. The saddle-node bifurcation point given in Eq. (17) is marked by a blue dot. The triangle indicates the scaling predicted by Eq. (16). [(c) and (d)] Same plots as in (a) and (b) for a finite system with volume $V_s = 1.8 \times 10^6 w^3$. The maximal droplet volume is $V_s \bar{\phi}^B$ in the passive system. The gray area in (d) denotes the region where systems are relatively small, $V_s \ll (4\pi/3)[D_B/(k_f + k_b)]^{3/2}$. In all panels, $\psi = 1$ and quantities are normalized to the length scale $w = 6\gamma\beta$ generated by the surface tension γ and the associated rate $k_0 = D_B/w^2$.

critical radius R_{crit} . This condition is violated if the reaction rates are too fast and droplets will shrink and disappear in this case. Consequently, there exist upper bounds for the rate constants above which droplets are not stable. To illustrate this, we vary the forward rate constant k_f while keeping the ratio k_f/k_b (and thus also the average volume fraction ϕ_0^B) fixed. In this case, droplets do not form if k_f exceeds the critical value k_f^c given by

$$k_f^c = \frac{4D_B}{(3\gamma\beta)^2} \frac{(\phi_0^B)^4}{1 - \phi_0^B}, \quad (17)$$

which follows from considering Eq. (13) in steady state.

Equation (13) is valid for droplets that are small compared to the characteristic length $l = [D_B/(k_f + k_b)]^{1/2}$, as discussed above in Sec. II C. Therefore, Eq. (16) is only valid if $\bar{R}/l = (3k_f/k_b)^{1/2} \ll 1$ or, alternatively, $\phi_0^B \ll 1/4$. This condition corresponds to the case of B -rich droplets in an A -rich background. In the opposite case of a large average volume fraction of B , $\phi_0^B \gg 3/4$, the system forms A -rich droplets in a B -rich background. These A -rich droplets are described by the same theory and thus have the size given by Eq. (16) but with k_f and k_b interchanged. In the intermediate case, where components A and B exist in approximately equal

average volume fractions ($k_f \approx k_b$, $\phi_0^B \approx 1/2$), droplets may not form and the effective description of emulsions is not applicable. It has been reported that bicontinuous structures are then prevalent in the solutions to Eq. (3b) [22,23]. Since we are interested in the dynamics of emulsions, we only discuss the case where B -rich droplets form ($3k_f \ll k_b$, $\phi_0^B \ll 1/4$).

Taken together, droplets will grow indefinitely in passive, thermodynamically large systems. Conversely, first-order chemical reactions can stabilize single droplets if $k_f < k_f^c(\phi_0^B)$ and $\phi_0^B \ll 1/4$. Combining these two necessary conditions, the rate constant k_f must be much smaller than the rate $k_0 = D_B/w^2$ of diffusion across the interface for a single droplet to be stable.

2. Finite systems

We next discuss the case of a single droplet in a system of finite volume V_s . Here the average volume fraction ϕ_0^B in the background fluid changes with time, which influences the droplet growth. In fact, the droplet volume must be smaller than the volume $V_s \bar{\phi}^B$ of B components in the system.

In the passive case ($k_f = k_b = 0$), a single droplet grows until an equilibrium with the background fluid is achieved. For a finite system, this occurs at a finite droplet radius \bar{R} , see Fig. 3(c). In the limit of small surface tension and strong phase separation, the actual steady-state volume \bar{V} is very close to the upper bound and $\bar{V} \approx V_s \bar{\phi}^B$ is thus a good approximation. Note that the average volume fraction $\bar{\phi}^B$ of B in the system is constant in passive systems.

In the case with chemical reactions ($k_f > 0$, $k_b > 0$), there are two regimes for the droplet size, depending on how the system size $R_s = (3V_s/4\pi)^{1/3}$ compares to the characteristic length scale l generated by the reaction-diffusion system. In large systems ($R_s \gg l$), a droplet grows until it reaches the radius \bar{R} given by Eq. (16). Conversely, in small systems ($R_s \ll l$), the droplet depletes the background fluid of B components significantly and its volume can be approximated by $\bar{V} \approx V_s \bar{\phi}^B$, where $\bar{\phi}^B = k_f/(k_f + k_b)$. These two regimes for the droplet size are observed in numerical solutions of the steady states, see Fig. 3(d).

B. Dynamics of multiple droplets

We next study the dynamics of systems containing several droplets. The dynamics of these droplets is coupled because they compete for the material in the background fluid.

1. Dynamics of a droplet pair in a finite system

We first discuss the qualitative behavior of a droplet pair in a finite system. Starting with two droplets of generally different volume, the initial dynamics are such that the combined droplet volume V_{tot} and the volume fractions in the background fluid approach their steady-state values quickly, see Appendix D. Apart from small corrections due to surface tension effects, V_{tot} is then given by the stationary volume that a single droplet would reach in the same system, which we discussed in the previous section. Droplet dynamics on longer times involves diffusive transport of material between the droplets, as in conventional emulsions [39].

In the passive case ($k_f = k_b = 0$), the material exchange between droplets is driven by diffusive fluxes which originate

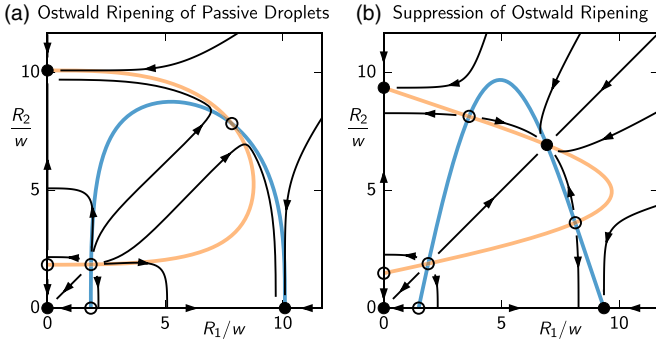


FIG. 4. (Color online) Behavior of two droplets as a function of their radii R_1 and R_2 . The black arrows indicate the temporal evolution of the state variables R_1 and R_2 following from Eq. (13), with ϕ_0^B given by Eq. (14) in steady state. The medium blue and light orange lines are the nullclines, which indicate where the growth rate of droplets 1 and 2 vanish, respectively. Their intersections are stable (disks) or unstable fixed points (open circles). (a) Passive system, $k_f = k_b = 0$, with $\bar{\phi}^B = 1/11$. (b) First-order reactions, $k_f/k_0 = 1.4 \times 10^{-4}$ and $k_b = 10k_f$. Model parameters are $\psi = 1$ and $V_s/w^3 = 5.8 \times 10^4$, where $w = 6\gamma\beta$ is the length scale generated by the surface tension γ .

from the differences in the volume fractions $\phi_+^B = \gamma\beta/R$ on the surface outside the droplets. In particular, ϕ_+^B is bigger for small droplets than for large droplets. Consequently, the diffusive material flux is directed from smaller droplets toward larger ones and thus amplifies initial size differences of droplets, a phenomenon called Ostwald ripening [8].

This behavior can be discussed most clearly by considering a droplet pair in the case where the background fluid described by Eq. (14) has reached a steady state. Figure 4 represents the dynamics of two droplet radii described by Eq. (13). Stable and unstable steady states are shown as full and open circles, respectively. An unstable steady state with two large droplets of equal size exists. In the vicinity of this state, one droplet grows at the expense of the other one. Additionally, there are three stable steady states, which have at most a single droplet, and there are three unstable steady states with small droplets, which are related to the critical radius R_{crit} . Passive droplets can thus grow if they start with a radius larger than R_{crit} , but at long times only a single droplet can be stable because of Ostwald ripening.

Importantly, Ostwald ripening can be suppressed if chemical reactions are occurring ($k_f > 0$, $k_b > 0$). In this case, the steady state with two coexisting large droplets of equal size can become stable as shown in Fig. 4(b). In the vicinity of this steady state, the smaller droplet grows at the expense of the larger one. In the case where Ostwald ripening is suppressed by chemical reactions, there are still stable steady states with a single droplet or even no droplets, see Fig. 4(b). Droplets have to overcome a critical radius in order to be able to grow. Note that the critical radius is similar to the one in the passive case. This is consistent with our result obtained for single droplets, see Fig. 3.

2. Stability conditions for multiple droplets

In order to discuss the stability condition for coexisting droplets of equal size, we consider the general case of N

droplets with same stationary radius \bar{R} . The value of \bar{R} depends on the number of droplet, the system size, and other parameters as discussed below. Starting from such a steady state, the stability of this state is governed by the slow exchange of material between the droplets, while the total droplet volume and the background fluid quickly reach their stationary state, see Appendix D. The slowest rate of relaxation to the steady state is given by

$$\lambda = \frac{D_B\gamma\beta}{\bar{R}^3} - \frac{2k_b}{3}, \quad (18)$$

see Appendix D. Note that λ is independent of the droplet count, because our effective theory only captures the mean-field coupling of the droplet dynamics. Importantly, λ can be either positive or negative. For $\lambda > 0$, the steady state is unstable and larger droplets grow at the expense of smaller droplets. In this case, the system exhibits Ostwald ripening and coarsens over time. For $\lambda < 0$, the steady state is stable and Ostwald ripening is suppressed.

In the passive case ($k_f = k_b = 0$), the characteristic rate simplifies to $\lambda = D_B\gamma\beta\bar{R}^{-3}$ [14]. Importantly, λ is positive and Ostwald ripening always occurs. Furthermore, systems with larger average droplet size coarsen slower, which is related to the well-known Lifshitz-Slyozov kinetics of droplet coarsening [39]. In order to verify Eq. (18), we simulate droplets by solving Eqs. (3) numerically and measure their coarsening rates, see Fig. 5(a) and Appendix E. Figure 5(b) shows that the analytical expression of λ can account for the observed coarsening in passive systems.

In the case of first-order reactions ($k_f > 0$, $k_b > 0$), the characteristic rate λ can become negative and the steady state with multiple droplets can be stable. In particular, λ is negative if the radius of the droplets is larger than the threshold value

$$R_{\text{stab}} = \left(\frac{3D_B\gamma\beta}{2k_b} \right)^{\frac{1}{3}}, \quad (19)$$

which follows from Eq. (18). Therefore, multiple droplets can be stable only if the stationary radius \bar{R} of the individual droplets is larger than R_{stab} . Whether this is the case depends on the droplet number density $n = N/V_s$.

In a state with low droplet density, $n \ll l^{-3}$, droplets do not influence the volume fractions in the background fluid significantly, and the droplet radius \bar{R} is given by Eq. (16). In this case, \bar{R} is indeed larger than R_{stab} , because k_f must be smaller than the critical value given in Eq. (17) for droplets to exist. Consequently, droplets are stable and Ostwald ripening is suppressed in this case.

In the case of a large droplet number density, $n \gg l^{-3}$, the stationary size of individual droplets is smaller as compared to the low-density system. This is because the total droplet volume is limited by the total volume $V_s\bar{\phi}^B$ of droplet material in the system, where $\bar{\phi}^B = k_f/(k_f + k_b)$. Using the estimate $V_s\bar{\phi}^B$ for the volume of a single droplet in a small system and considering that this volume must be distributed among the N droplets, we have

$$\bar{V} \approx \frac{k_f V_s}{(k_f + k_b)N}. \quad (20)$$

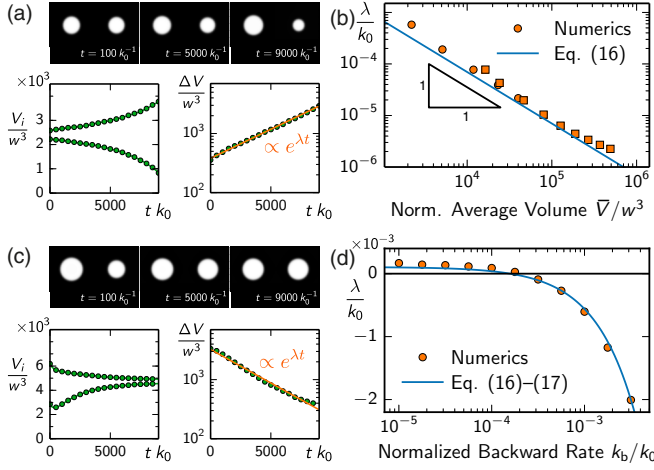


FIG. 5. (Color online) Numerical simulations of the dynamics of two droplets. (a) Illustration of the numerical procedure for a passive system ($k_f = k_b = 0$, $\bar{\phi}^B = 1/11$). We numerically solve Eq. (3) in a cylindrical geometry as described in Appendix E. Snapshots (top panel) are used to measure the droplet volumes V_i as a function of time t (lower left panel). The rate λ is determined by a linear fit to the logarithm of the volume difference ΔV (lower right panel). (b) Coarsening rate λ as a function of the average droplet volume \bar{V} for $k_f = k_b = 0$ with $\bar{\phi}^B = 1/11$. The analytical prediction (solid line) given by Eq. (18) is compared to numerical results (symbols) for $V_s/w^3 = 1.5 \times 10^5$ (discs) and $V_s/w^3 = 1.2 \times 10^6$ (squares). (c) Same as (a) for $k_b/k_0 = 5 \times 10^{-3}$ and $k_f/k_0 = 5 \times 10^{-4}$. (d) Rate λ as a function of the backward rate constant k_b with $k_f = 0.1 k_b$. The analytical prediction given by combining Eqs. (18) and (20) (solid line) is compared to numerical results (orange disks) for $V_s/w^3 = 1.5 \times 10^5$.

The steady state of N droplets of size $\bar{R} = [3\bar{V}/(4\pi)]^{1/3}$ is stable if the corresponding relaxation rate λ given by Eq. (18) is negative. This is the case for sufficiently large rate constant k_b .

This change of stability as a function of the reaction rates is shown in Figs. 5(c) and 5(d), which display simulation results for two droplets with first-order reactions. These simulations show that the measured relaxation rates agree with the analytical expression of λ given in Eq. (18). We can thus use Eq. (18) to determine parameter values at which multiple droplets are stable. This can be summarized in a single dimensionless stability number,

$$\chi = \frac{V_s}{2\pi D_B \gamma \beta N} \cdot \frac{k_f k_b}{k_f + k_b}, \quad (21)$$

which is defined such that $\chi > 1$ corresponds to $\lambda < 0$ for the droplet volume given by Eq. (20). Consequently, a steady state with N droplets is stable if χ is larger than 1. Equation (21) thus allows us to estimate the maximal number N_{\max} of droplets that can be stable at given parameter values. Generally, more droplets can be stable for faster chemical reactions and the estimate following from the condition $\chi > 1$ agrees well with numerical results, see Fig. 6(a). However, droplets cannot be stable for rate constants k_f above the maximal rate k_f^c given in Eq. (17). The value of N_{\max} thus vanishes as this point is approached, see Fig. 6(a).

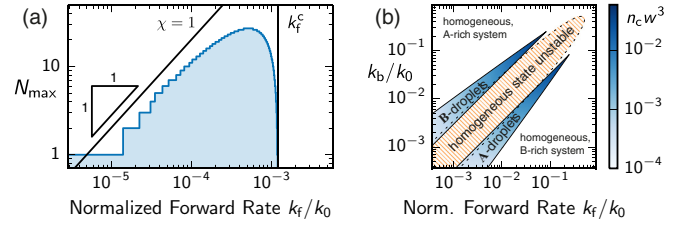


FIG. 6. (Color online) Stability of multiple droplets with first-order reactions. (a) The maximal number N_{\max} of stable droplets (blue line) as a function of the forward reaction rate constant k_f with $k_b = 10 k_f$ in a finite system of volume $V_s = 2.3 \times 10^5 w^3$. N_{\max} is obtained from a numerical linear stability analysis of Eq. (13). The theoretical stability boundaries $\chi = 1$ (left black line) given by Eq. (21) and $k_f = k_f^c$ (right black line) given by Eq. (17) are indicated. (b) Stability of possible states in an infinite system as a function of the reaction rate constants k_f and k_b . The homogeneous state $\phi^B(\mathbf{r}) = \phi_0^B$ with $\phi_0^B = k_f/(k_f + k_b)$ is unstable and bicontinuous structures typically form in the orange hatched region bounded by the stability condition given in Appendix F (dashed line). Droplets enriched in B components are stable in the upper blue region, which is defined by $3k_f < k_b < 16k_0(\phi_0^B)^3$, following from Eq. (17). The color indicates the maximal droplet density n_c , which follows from Eq. (21) for $\chi = 1$. Correspondingly, A -rich droplets are stable in the lower blue region. The homogeneous state $\phi^B(\mathbf{r}) = \phi_0^B$ is the only stable state in the white region.

3. Stability of multiple droplets in large systems

In passive systems, droplets undergo Ostwald ripening with the typical Lifshitz-Slyozov kinetics, where the mean droplet radius $\langle R \rangle$ evolves as $\langle R \rangle \propto (t D_B/w^2)^{1/3}$ [39]. In the case where first-order reactions are occurring, we find that the behavior depends on the number density $n = N/V_s$ of droplets in the system. In the case where n is larger than a critical value n_c following from Eq. (21) for $\chi = 1$, large droplets grow and smaller ones disappear until n falls below n_c . If $n < n_c$, the system evolves toward a stable steady state in which all droplets have the same size. The size of these stationary droplets depends on the number density n . If the density is low, $n \ll l^{-3}$, the size of each droplet is given by Eq. (16). For larger number densities, $l^{-3} \ll n < n_c$, droplets are smaller than in the case of low n and their size is given by Eq. (20). Note that faster chemical reactions typically lead to a larger n_c , but droplets cannot be stable beyond the critical reaction rate given by Eq. (17). This is illustrated in Fig. 6(b), which shows the parameter region in which B -rich droplets are stable. The figure also shows the corresponding region of stable, A -rich droplets. Between these two regions, the homogeneous state is unstable, see Appendix F. Consequently, structures form spontaneously and critical droplet radii do not exist. In fact, bicontinuous structures have been reported for the symmetric case $k_f = k_b$ [22,23].

IV. AUTOCATALYTIC DROPLETS

So far, we considered droplet dynamics under the influence of first-order reactions. In the context of biology, chemical reactions are usually more complex. In this section, we study an autocatalytic system in which the droplet material serves as a catalyst for its own production. One interesting

aspect of autocatalytic systems is that droplets are difficult to nucleate, because droplet material can be produced only from preexisting droplet material. We therefore introduce active cores that catalyze the production of droplet material and can nucleate autocatalytic droplets. Such a system can serve as a model for the growth of centrosomes [5].

Autocatalytic systems are typically unstable when binary fluids are considered. This is because the entire system can be turned into droplet material by the autocatalytic reaction. We thus discuss autocatalytic droplets in the framework of ternary fluids with a nonreactive component C introduced in Sec. II.

For an autocatalytic droplet of radius R_i , the growth rate of the droplet volume V_i reads

$$\frac{dV_i}{dt} = \frac{4\pi D_B}{\psi} (\phi_0^B R_i - \gamma\beta) + V_i \left(\frac{k_s \phi_0^A}{\psi} - k_b \right) + \frac{Q_i \phi_0^A}{\psi}, \quad (22)$$

where $k_s = k_f + k\psi$, see Eq. (9). This equation is accompanied by Eqs. (10) and (12), which describe the dynamics of the volume fractions ϕ_0^A and ϕ_0^B outside of droplets.

A. Dynamics of a single autocatalytic droplet

We first investigate a single, autocatalytic droplet ($k_f = 0$, $k_b > 0$, $k > 0$, $Q = 0$), see Fig. 2(b). In systems with a finite volume V_s , such a droplet can reach a stationary state with a volume \bar{V} . This volume is smaller than the system size and reads

$$\bar{V} \approx \frac{V_s}{\psi} \left(\bar{\phi} - \frac{k_b}{k} \right), \quad (23)$$

which is valid for small surface tension, see Appendix B. This expression shows that a sufficiently fast autocatalytic rate is required ($k > k_b/\bar{\phi}$) for droplets to grow. Note that the stationary volume \bar{V} scales with the system size and that the autocatalytic reaction does not set a characteristic droplets size, in contrast to the first-order reactions discussed above. Autocatalytic droplets thus behave more like passive droplets, which also grow up to a certain fraction of the system size.

Similarly to the previously discussed systems, an autocatalytic droplet only grows if it is larger than a critical radius R_{crit} , see Fig. 7(a). This critical radius can be estimated by $R_{\text{crit}} \approx \gamma\beta/\phi_0^B$, where the fraction ϕ_0^B in the background fluid is given by $\phi_0^B = \bar{\phi} - k_b/k$. Thus, the critical radius diverges if $k = k_b/\bar{\phi}$, where droplets no longer grow. In an autocatalytic system, the volume fraction ϕ_0^B of droplet material B is lower than in a passive system and the critical radius is larger. Droplets in autocatalytic systems are thus harder to nucleate than in passive systems.

Interestingly, nucleation can be facilitated and even triggered reliably by an active core, which catalyzes the production of droplet material B . The critical radius vanishes for a large-enough catalytic activity Q , see Fig. 7(a). Consequently, nucleation around an active core is guaranteed if Q is larger than a critical value Q_c . Considering Eq. (22) in the steady state for small droplets, we obtain $Q_c \approx 4\pi D_B \gamma\beta/\phi_0^A$ with $\phi_0^A = k_b/k$ following from Eq. (10) for $k_f = 0$. Importantly, catalytically active cores strongly influence the nucleation behavior of autocatalytic droplets, but their effect on the steady state size is small, see Fig. 7 and Appendix B.

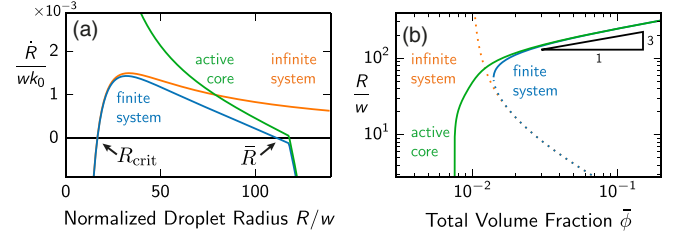


FIG. 7. (Color online) Behavior of a single autocatalytic droplet in an infinite system (orange; $Q_1 = 0$), in a finite system (blue; $V_s/w^3 = 6.9 \times 10^7$, $Q_1 = 0$), and in a finite system with a catalytically active core (green; $V_s/w^3 = 6.9 \times 10^7$, $Q_1 = 300 w^3 k_0$). (a) Growth rate $\dot{R} = dR/dt$ derived from Eq. (22) as a function of the droplet radius R for $\bar{\phi} = 0.02$. The critical radius R_{crit} and the stable radius \bar{R} derived from Eq. (23) are indicated. (b) Bifurcation diagram of the droplet radius as a function of the total volume fraction $\bar{\phi}$ of material. Dotted lines indicate unstable steady states. Model parameters are $k/k_0 = 0.02$, $k_b/k_0 = 2 \times 10^{-4}$, and $\psi = 0.1$, with $k_0 = D_B/w^2$.

B. Dynamics of multiple autocatalytic droplets

We next study the dynamics of systems containing several autocatalytic droplets. In the simple case without catalytic cores ($Q_i = 0$), large droplets grow at the expense of smaller droplets and states with multiple droplets are unstable. This can be seen explicitly by considering two autocatalytic droplets in a finite system.

This system possesses a steady state with two large droplets of the same size, which is unstable, see Fig. 8(a). In fact, at most a single droplet can be stable in this system. Furthermore, there are critical radii, which droplets have to overcome in order to grow. Consequently, the dynamics of two autocatalytic droplets is qualitatively very similar to two droplets in a passive system, compare Fig. 4(a) and Fig. 8(a). In contrast

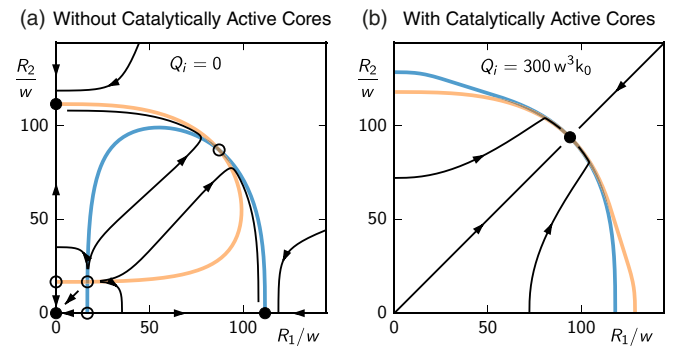


FIG. 8. (Color online) Behavior of two autocatalytic droplets as a function of their radii R_1 and R_2 . The black arrows indicate the temporal evolution of the state variables R_1 and R_2 following from Eq. (22). The medium blue and light orange lines are the nullclines, which indicate where the growth rate of droplets 1 and 2 vanish, respectively. Their intersections are stable (disks) or unstable fixed points (open circles). (a) No cores, $Q_i = 0$. (b) Catalytically active cores, $Q_i = 300 w^3 k_0$. The volume fractions ϕ_0^A and ϕ_0^B are fixed to their stationary state value and model parameters are $k_f = 0$, $k_b/k_0 = 2 \times 10^{-4}$, $k/k_0 = 0.02$, $\psi = 0.1$, $\bar{\phi} = 0.02$, and $V_s/w^3 = 6.9 \times 10^7$.

to the reactions with first-order kinetics discussed above, the autocatalytic reaction thus does not suppress Ostwald ripening.

Interestingly, the two autocatalytic droplets can be stabilized by catalytically active cores ($Q_i > 0$), see Fig. 8(b). In the shown case of equal catalytic activity, $Q_1 = Q_2 = 300w^3k_0$, the smaller droplet grows at the expense of the larger droplet until both droplets reached the same size. This is because the material influx caused by an active core is more important for small droplets than for large ones and thus promotes the growth of small droplets. Thus, for sufficiently large Q , the small droplet can grow at the expense of the large droplet until both have the same stable size. Interestingly, there are no critical radii in this case and the single stable state is reached from all initial conditions. This is because the catalytically active cores not only stabilize the two droplets but they also trigger their nucleation, as discussed above. Consequently, the number of stable droplets will be set by the number of active cores.

These results can be generalized to multiple droplets with catalytic cores of equal activity ($k_f \geq 0$, $k_b \geq 0$, $k \geq 0$, $Q_i = Q \geq 0$). A linear stability analysis of Eq. (22) reveals that the total droplet volume V_{tot} and the volume fractions ϕ_0^A and ϕ_0^B in the background fluid quickly reach their steady-state values, while droplets exchange material on a slower time scale, similarly to the case of a binary fluid discussed above. The rate λ at which droplets exchange material reads

$$\lambda \approx \frac{4\pi D_B \gamma \beta}{3\psi \bar{V}} + \frac{2J}{3\psi \bar{V}} - \frac{Q}{\bar{V}k} \left(k_b + \frac{J}{\psi \bar{V}} \right), \quad (24)$$

where J is given by Eq. (11) for $R_i = \bar{R}$. The rate λ corresponds to the slowest relaxation time to reach a steady state with multiple droplets of equal volume \bar{V} for fixed ϕ_0^A and ϕ_0^B , see Appendix G. A steady state with multiple droplets is stable if λ is negative, which is the case either for a large flux of B components into the droplets, $J < 0$, or for large Q . These cases correspond to fast first-order reactions and strong active cores, respectively. In particular, we find Eq. (18) for $\psi = 1$ in the case of first-order reactions ($k_f > 0$, $k_b > 0$, $k = 0$, $Q = 0$), where $J = -k_b \psi \bar{V}$.

In the case of an autocatalytic reaction ($k_f = 0$, $k_b > 0$, $k > 0$, $Q \geq 0$) droplet material B is predominately produced inside droplets. In the stationary state, this production is balanced by a small efflux $J > 0$ of droplet material. This droplet material is then recycled into soluble building blocks outside of droplets. This process leads to a small volume fraction $\phi_0^B < \phi_+^B$, where we have $\phi_0^B \approx \phi_+^B$ in small systems ($V_s/N \ll l^3$) and $\phi_0^B \approx 0$ in large systems ($V_s/N \gg l^3$), with $l = (D_B/k_b)^{1/2}$. Because of the constant efflux of droplet material, autocatalytic droplets without a catalytic core ($Q = 0$) will coarsen even faster than droplets in a passive system, compare Eqs. (24) and (18). In particular, the coarsening should be fastest in large systems, where J is maximal. In order to test this prediction, we measure λ from numerical solutions of Eqs. (3), see Fig. 9(a). Indeed, both smaller droplets and larger systems lead to faster coarsening and Eq. (24) gives a good estimate of λ . Importantly, the rate λ is always positive, indicating that autocatalytic droplets are unstable and exhibit Ostwald ripening.

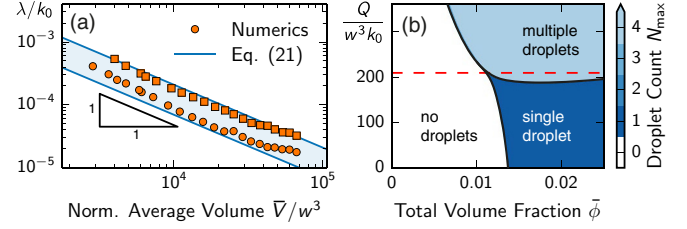


FIG. 9. (Color online) Behavior of emulsions of autocatalytic droplets. (a) Rate λ as a function of the average droplet volume \bar{V} . The analytical prediction given by Eq. (24) for small systems ($\phi_0^B = \phi_+^B$, lower blue line) and large systems ($\phi_0^B = 0$, upper blue line) is compared to numerical results for small (orange disks, $V_s/w^3 = 1.5 \times 10^5$) and large (orange squares, $V_s/w^3 = 8.8 \times 10^5$) systems, which were obtained as described in Fig. 5. Model parameters are $\psi = 0.1$, $k/k_0 = 100$, $k_b/k_0 = 0.01$. (b) Maximal number N_{max} of stable droplets as a function of the total volume fraction $\bar{\phi}$ of material and the catalytic activity Q_i of cores within the droplets. The red dashed line denotes the approximate threshold value of Q_i given in Eq. (25) with $\phi_0^B \approx 0$ valid for large systems. Model parameters are $\psi = 0.1$, $k/k_0 = 0.02$, $k_b/k_0 = 2 \times 10^{-4}$, $V_s/w^3 = 6.9 \times 10^7$.

Ostwald ripening of autocatalytic droplets can be suppressed by catalytically active core ($Q > 0$), see Fig. 8(b). In particular, autocatalytic droplets are stable if Q exceeds the threshold value

$$Q_{\text{stab}} \approx \frac{4\pi D_B k_s R (3\phi_+^B - 2\phi_0^B)}{3\psi k_b}, \quad (25)$$

which follows from Eq. (24). Note that Q_{stab} becomes independent of the droplet radius R in the case of large systems where $\phi_0^B \approx 0$. Figure 9(b) shows that there is a critical value Q_{stab} above which multiple droplets are stable. Equation (25) gives a good estimate for this threshold if the average fraction $\bar{\phi}$ is large enough. Generally, the stability threshold Q_{stab} is larger than the critical activity Q_c that is required for droplet nucleation. This can be seen by considering Eq. (25) in the limit $\phi_0^B \approx 0$ in the parameter regime where droplets form ($k > k_b/\bar{\phi}$). Consequently, catalytically active cores that are strong enough can both nucleate and stabilize autocatalytic droplets.

Finally, we consider autocatalytic droplets with cores of unequal catalytic activities ($k_f = 0$, $k_b > 0$, $k > 0$, $Q_i > 0$). In this case, the droplet around the core with stronger catalytic activity grows faster, see Eq. (22). This difference in the growth rates can be observed in the simple case of two droplets, see Fig. 10(a). The figure shows that both catalytic cores nucleate droplets and that the droplet with larger core activity grows more quickly. Similarly to the two droplets with equal catalytic cores shown in Fig. 8(b), there is a single stable steady state, which is reached from all initial conditions. However, contrary to the symmetric system, the steady-state droplet volumes are not equal, but the droplet with the core with higher activity becomes larger. This can be understood by considering the growth rates given in Eq. (22) in the simple case of vanishing surface tension γ . In this case, the fraction ϕ_0^B of droplet material in the background fluids vanishes, see Eq. (10), and the ratio of the two droplet volumes is determined by the ratio of their catalytic activities. Note that if only one of the

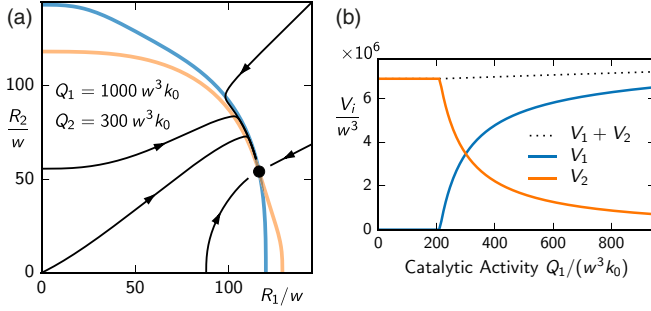


FIG. 10. (Color online) Behavior of two autocatalytic droplets with cores of unequal activity Q_i . (a) Temporal evolution of the droplet radii R_1 and R_2 (black lines) following from Eq. (22) for $Q_1 = 1000 w^3 k_0$ and $Q_2 = 300 w^3 k_0$. The medium blue and light orange lines are the nullclines, which indicate where the growth rate of droplets 1 and 2 vanish, respectively. Their intersection (disk) is the only fixed point, which is stable. (b) Droplet volumes V_i in steady state as a function of the catalytic activity Q_1 of one core for $Q_2 = 300 w^3 k_0$. In both panels, ϕ_0^A and ϕ_0^B are fixed to their stationary state values and model parameters are $k_f = 0$, $k_b/k_0 = 2 \times 10^{-4}$, $k/k_0 = 0.02$, $\psi = 0.1$, $\bar{\phi} = 0.02$, and $V_s/w^3 = 6.9 \times 10^7$.

catalytic activities is larger than Q_{stab} while the other one is smaller, only a single droplet is stable, see Fig. 10(b). The catalytic cores thus can determine how the droplet material is distributed among the droplets, but they only have a weak effect on the total droplet volume, which is still well approximated by Eq. (23).

This behavior has been observed in experiments on centrosomes, which can be described as autocatalytic droplets with active cores [5]. In this case two cores of equal catalytic activities occur. However, experiments in which one core is perturbed lead to unequal centrosomes which can be understood as a result of unequal catalytic activities [5].

V. DISCUSSION

In practical terms Ostwald ripening inhibits the use of liquid droplets in many circumstances. This is because larger droplets tend to grow at the expense of smaller droplets. As a result, droplets size varies and is hard to control. Therefore, it is very important to find mechanisms that suppress the ripening of such liquid emulsions. In this work we demonstrate that emulsions can be stabilized if the constituents of the phase separating fluids are converted into each other by nonequilibrium chemical reactions.

The stability of active emulsions depends on the rate of the chemical reactions. In the limit of vanishing reaction rates, Eq. (3b) reduces to the Cahn-Hilliard equation, such that the active emulsions behave like their classical, passive counterparts and undergo Ostwald ripening [33,38]. For intermediate reaction rates, Ostwald ripening is typically suppressed and multiple droplets are stable. Large reaction rates lead to the breakup of droplets.

In the simple case of first-order reactions, droplet material is produced outside of droplets and converted back into soluble building blocks inside the droplets. This causes a material influx that scales with the droplet radius R , see Eq. (11), while the efflux scales with the droplet volume $V \propto R^3$, see

Eq. (9). Consequently, large droplets have a tendency to shrink, because the material efflux dominates the influx. The influx and efflux are balanced at a specific droplet size at which droplets are stationary. This stationary droplet size depends on the chemical reaction rates.

Interestingly, we show in this case that the droplet radius above which multiple droplets are stable is proportional to $k_b^{-1/3}$, see Eq. (19). Note that in the symmetric case $k_f = k_b$ the same scaling was also found for the length scale of bicontinuous structures [22] and for concentric circular patterns [28]. We find an additional scaling regime in the case of small droplet densities, where the stable radius is proportional to $k_b^{-1/2}$ for constant k_f/k_b , see Eq. (16). In both scaling regimes, the droplet size in the active emulsion can be controlled by adjusting the rate constants of the first-order reactions.

Our theory can also be applied to systems with more complex chemical reactions. As an example, we consider the case of second-order autocatalytic reactions, where droplets produce their own material. These autocatalytic droplets can grow at rapidly increasing rates until they have used up the material provided in their environment. In the steady state, the material fluxes are then opposite to those in the case of first-order reactions. Because of this, Ostwald ripening occurs at rates that can be even larger than in systems without chemical reactions. Furthermore, autocatalytic droplets are difficult to nucleate, because they require preexisting droplet material to grow.

Our analysis shows that Ostwald ripening can be suppressed in autocatalytic droplets if catalytic cores are introduced. This is because the catalytic activity facilitates the growth of small droplets while having little effect on large droplets. Active cores therefore allow the control of stability, nucleation behavior, and the relative size of autocatalytic droplets, while the sum of all droplet volumes is mainly determined by the conserved total volume of A and B components in the system.

Our work shows that first-order chemical reactions or second-order reactions with active cores allow for emulsions in which several droplets are stable. The concept of autocatalytic droplets with catalytic cores has been exploited to account for the growth behaviors of centrosomes [5]. Centrosomes are collections of proteins that are required for cell division. It is important for correct cell division that each cell contains two centrosomes of the same size. Although it has long been known that centrosomes grow from centrioles, it has been unclear how centrioles control nucleation and growth of centrosomes. Our work suggests that centrioles act as active cores nucleating and stabilizing the growth of centrosomes, thereby suppressing Ostwald ripening and leading to two centrosome droplets of equal size in the cell that coexist during cell division.

More generally, recent work has shown that cells contain chemically distinct compartments that form and are maintained by liquid-liquid demixing [4]. Examples are P granules and nucleoli among others, which can be viewed as liquidlike droplets in the cell [40]. In each of these cases the number and size of droplets is probably controlled by the cell, which could be done using the effects of chemical reactions discussed here. Furthermore, droplet dynamics associated with size control and the turnover of the constituents may play a role in preventing droplets to turn into stable protein aggregates,

which are often linked to diseases [41]. It will be interesting to see whether the principles enunciated in this paper apply to these and other liquidlike compartments in cells.

Controlling the properties of emulsions is also important in many technological applications. It would thus be interesting to conduct experiments where Ostwald ripening is suppressed by chemical reactions. As we show here, these reactions must be driven away from equilibrium, which could be achieved, for example, by driving photochemical reactions by light [21,42]. Alternatively, a system could be coupled via a semipermeable membrane to a source of fast-diffusing fuel molecules that drive the chemical reactions between the droplet components.

Active emulsions stabilized by chemical reactions are an example of pattern formation far from equilibrium. There is some similarity with the formation of Turing patterns in reaction-diffusion systems [43]. Note, however, that our work generalizes the concept of Turing patterns by combining conventional phase coexistence with chemical pattern formation. In this case, spatial patterns stemming from reactions and diffusion of chemical species are combined with the formation of distinct phases by physical interactions between molecules. The interfaces of chemically active droplets are thus related to thermodynamics and very different from interface-like structures in Turing patterns. As a consequence, the systems described in this manuscript can exhibit stable emulsions in parameter regions in which conventional reaction-diffusion systems would not form patterns.

Ostwald ripening can also be suppressed by other nonequilibrium mechanisms like shearing the fluid continuously [17,18]. However, while shearing drives the system from the boundary, our system breaks detailed-balance locally and thus belongs to the class of active matter. The advantage of our system is that it reaches a stationary state with spherical droplets of a well-defined size. Such uniform emulsions can also be stabilized by inclusion of additional components inside droplets, which are insoluble in the background fluid [16]. However, large droplets, which could, for instance, form due to droplet coalescence, would still grow and Ostwald ripening might still happen in such systems. In contrast, our theory predicts that all large droplets are unstable and shrink back to the single stable size. In our model, emulsions thus can be stable despite large fluctuations caused by droplet coalescence and droplet nucleation. These effects will merely broaden the droplet size distribution.

The precise influence of droplet coalescence in our model can only be studied if it is extended to take into account hydrodynamic effects, which are known to influence the dynamics of reactive binary mixtures [44,45]. Such an extended theory may also be necessary to compare predicted droplet sizes and rates of growth dynamics to experiments, where fluid convection and Brownian motion of droplets are hard to eliminate. Moreover, adding hydrodynamics would allow us to study the interaction of active droplets.

ACKNOWLEDGMENTS

We thank Christoph Weber and Rabea Seyboldt for helpful discussions and a critical reading of the manuscript. F.J. and A.A.H. acknowledge funding from the European Commu-

nity's Seventh Framework Programme (FP7/2007-2013) grant agreement 241548 (MitoSys Project).

APPENDIX A: COEXISTENCE IN A TERNARY FLUID

The conditions for equilibrium at the interface between two coexisting phases read

$$0 = \mu^A(\phi_-^A, \phi_-^B) - \mu^A(\phi_+^A, \phi_+^B), \quad (\text{A1a})$$

$$0 = \mu^B(\phi_-^A, \phi_-^B) - \mu^B(\phi_+^A, \phi_+^B), \quad (\text{A1b})$$

$$0 = (\phi_-^A - \phi_+^A)\mu^A(\phi_-^A, \phi_-^B) + (\phi_-^B - \phi_+^B)\mu^B(\phi_-^A, \phi_-^B) + f(\phi_+^A, \phi_+^B) - f(\phi_-^A, \phi_-^B) - 2\gamma H, \quad (\text{A1c})$$

where ϕ_-^i and ϕ_+^i for $i = A, B$ denote the volume fractions at the interface inside and outside the droplet, respectively. Here $\mu^i(\phi^A, \phi^B) = \partial f(\phi^A, \phi^B) / \partial \phi^i$, γ denotes the surface tension, and H is the mean curvature of the interface, with $H = R^{-1}$ for a sphere of radius R . For the free energy density given in Eq. (1), Eq. (A1a) yields $\phi_+^A = \phi_-^A$. The volume fractions of B , which result from Eqs. (A1), can be expanded to first order in H :

$$\phi_-^B \approx \psi + \beta\gamma H \quad \text{and} \quad \phi_+^B \approx \beta\gamma H, \quad (\text{A2})$$

where $\beta = 2/(b\psi)$. Equation (A2) also holds for binary fluids ($\phi^C = 0$), where the volume fraction of building blocks is given by $\phi_\pm^A = 1 - \phi_\pm^B$.

APPENDIX B: AUTOCATALYTIC DROPLETS AT STEADY STATE

We consider a single, autocatalytic droplet of radius R with an infinitely thin interface ($k > 0$, $k_b > 0$, $k_f = 0$, $Q_i = 0$). Away from the interface, the volume fractions $\phi^A(\mathbf{r})$ and $\phi^B(\mathbf{r})$ are governed by the reaction-diffusion system given in Eqs. (7). For simplicity, we consider a spherically symmetric system around the droplet. Inside the droplet ($r < R$), we have the boundary conditions $\phi^A(R) = \phi_0^A$ and $\phi^B(R) = \psi$, see Eq. (6), and the steady-state solution to Eqs. (7) thus reads $\phi^A(r) = k_b/k$ and $\phi^B(r) = \psi$ in this region. Outside of the droplet ($r > R$), we have $\phi^A(r) = k_b/k$ and $\phi^B(r) = \gamma\beta/R$. Importantly, the volume fraction $\phi^B(r)$ is homogeneous inside the droplet. Note that this argument also holds for states with multiple droplets and the contribution of the autocatalytic reaction to the typical length scale l thus can generally be neglected.

We next discuss the steady state of a single autocatalytic droplet including surface tension effects, $\gamma > 0$, and catalytically active cores, $Q > 0$. For small droplets ($R \ll l$), the dynamics of a single autocatalytic droplet in a finite system are described by Eq. (22) together with Eqs. (10) and (12). In the steady state, the droplet absorbs almost all droplet material B , such that the average volume fraction ϕ_0^B in the background fluid is negligible, $\phi_0^B = 0$. In this case, we can solve Eq. (12) for ϕ_0^A . Inserting this solution into Eq. (22) in steady state leads to a quadratic equation for the stationary droplet volume. Only keeping the linear contributions of the catalytic activity Q and the surface tension γ , the solution corresponding to the stable

droplet reads

$$\bar{V} \approx \frac{V_s}{\psi} \left(\bar{\phi} - \frac{k_b}{k} \right) + \frac{Qk_b^2 - 4\pi D_B k^2 \bar{\phi} \gamma \beta}{(k\bar{\phi} - k_b)kk_b\psi}. \quad (\text{B1})$$

The second solution to the quadratic equation is unstable and corresponds to the critical radius.

APPENDIX C: SURFACE FLUXES OF DROPLET MATERIAL

We can obtain a simplified expression for the flux $J = -4\pi R^2 D_B \phi^B(R)$ of droplet material at the droplet interface for steady states of the volume fraction $\phi^B(r)$ in a spherical geometry. At the droplet interface at $r = R$, we have $\phi^B(R) = \phi_+^B(R)$. For large $r \gg R$, $\phi^B(r)$ approaches the bulk volume fraction ϕ_0^B . Using Eq. (7b) with a vanishing time derivative, we have

$$\phi^B(r) = \phi_0^B + (\phi_+^B - \phi_0^B) \frac{R}{r} e^{(R-r)/l}, \quad (\text{C1})$$

where $l = [D_B/(k_f + k_b)]^{1/2}$ is a characteristic length and we neglected the autocatalytic reaction outside the droplet where ϕ^B is small. The flux J at the interface is then given by Eq. (11).

APPENDIX D: STABILITY ANALYSIS OF BINARY EMULSIONS

The dynamics of an emulsion of N droplets with first-order kinetics are given by Eqs. (13) and (14). These equations have a steady state where all droplets have the same radius \bar{R} and the volume fraction of droplet material in the background fluid is given by $\bar{\phi}_0^B$. The stability of this state can be investigated by considering small perturbations $R_i(t) = \bar{R} + \hat{R}_i(t)$ and $\phi_0^B(t) = \bar{\phi}_0^B + \hat{\phi}_0^B(t)$ with $\hat{R}_i \ll \bar{R}$ and $\hat{\phi}_0^B \ll \bar{\phi}_0^B$. The associated dynamics to linear order read

$$\frac{d\hat{R}_i}{dt} = D_B \left(\frac{\hat{\phi}_0^B}{\bar{R}} - \frac{\bar{\phi}_0^B \hat{R}_i}{\bar{R}^2} + \frac{2\gamma\beta \hat{R}_i}{\bar{R}^3} \right) - \frac{k_b \hat{R}_i}{3}, \quad (\text{D1})$$

$$\frac{d\hat{\phi}_0^B}{dt} = -(k_f + k_b) \hat{\phi}_0^B - \frac{4\pi D_B}{V_s} \sum_{i=1}^N (\bar{R} \hat{\phi}_0^B + \bar{\phi}_0^B \hat{R}_i). \quad (\text{D2})$$

Defining a vector \mathbf{X} with $X_0 = \hat{\phi}_0^B$ and $X_i = \hat{R}_i$ for $i = 1, \dots, N$, this can be written as $dX_i/dt = \sum_j \mathcal{J}_{ij} X_j$, where the components of the Jacobian \mathcal{J} are

$$\mathcal{J}_{00} = -k_f - k_b - 4\pi D_B N \bar{R} V_s^{-1}, \quad (\text{D3a})$$

$$\mathcal{J}_{0i} = -4\pi D_B N \bar{\phi}_0^B V_s^{-1}, \quad (\text{D3b})$$

$$\mathcal{J}_{i0} = D_B \bar{R}^{-1}, \quad (\text{D3c})$$

$$\mathcal{J}_{ii} = D_B \left(\frac{2\gamma\beta}{\bar{R}^3} - \frac{\bar{\phi}_0^B}{\bar{R}^2} \right) - \frac{k_b}{3}, \quad (\text{D3d})$$

$$\mathcal{J}_{ij} = 0, \quad (\text{D3e})$$

where $i \neq j$ and $i, j \geq 1$. The eigenvalues e of \mathcal{J} read

$$e_{\pm} = \frac{1}{2} [\mathcal{J}_{00} + \mathcal{J}_{ii} \pm \sqrt{(\mathcal{J}_{00} - \mathcal{J}_{ii})^2 + 4N \mathcal{J}_{0i} \mathcal{J}_{i0}}], \quad (\text{D4a})$$

$$\tilde{e} = \mathcal{J}_{ii}, \quad (\text{D4b})$$

where the eigenvalue \tilde{e} has multiplicity $N - 1$ and only exist for systems with multiple droplets, $N \geq 2$. The eigenvalues are ordered, $e_- < e_+ < \tilde{e}$, since $\mathcal{J}_{0i} \mathcal{J}_{i0} < 0$ and $\mathcal{J}_{00} < \mathcal{J}_{ii}$. This can be seen by rewriting Eq. (D3d) as $\mathcal{J}_{ii} = \gamma\beta D_B \bar{R}^{-3} - 2k_b/3$, where we used $\bar{\phi}_0^B$ resulting from solving Eq. (13) in steady state. Consequently, a system with multiple droplets can be stable only if $\tilde{e} < 0$ and it is thus sufficient to discuss the value of \mathcal{J}_{ii} , see Eq. (18). Note that the eigenspace associated with \tilde{e} describes dynamics where both ϕ_0^B and V_{tot} are constant and droplets merely exchanged material with each other.

APPENDIX E: NUMERICAL CALCULATIONS

We study the dynamics of two droplets in a finite system by numerically solving Eq. (3) in a three-dimensional, cylindrical geometry. Starting with an initial configuration that represents two droplets of slightly different volume, we determined the temporal dynamics using the XMDS2 framework [46] with an adaptive Runge-Kutta-Fehlberg time stepper and an implementation of the spatial derivatives using a spectral method with 128 and 32 support points in the axial and radial direction, respectively. The coarsening rate λ is then determined by a linear fit to the logarithm of the difference of the two droplet volumes, which are determined from the volume fraction fields.

APPENDIX F: STABILITY OF THE HOMOGENEOUS STATE

The dynamics of the volume fraction $\phi^B(\mathbf{r}, t)$ of a binary fluid with first-order chemical reactions ($k_f > 0, k_b > 0, k = 0, Q_i = 0$) are given by Eq. (3b) together with the free energy density $f(\phi^B) = \frac{b}{2}(\phi^B)^2(1 - \phi^B)^2$. The only homogeneous stationary state is $\phi^B(\mathbf{r}) = \phi_0^B$ with $\phi_0^B = k_f/(k_f + k_b)$. Perturbations of this state grow with a rate

$$\lambda(\mathbf{q}) = 2D_B \mathbf{q}^2 \left[\frac{4k_f k_b - k_f^2 - k_b^2}{(k_f + k_b)^2} - \frac{w^2}{8} \mathbf{q}^2 \right] - k_f - k_b, \quad (\text{F1})$$

where \mathbf{q} denotes the wave vector of the perturbation mode. The state $\phi^B(\mathbf{r}) = \phi_0^B$ is unstable if there exists a \mathbf{q} for which $\lambda > 0$. This is the case if

$$|k_f - k_b| < \frac{k_f + k_b}{\sqrt{3}} \sqrt{1 - w \sqrt{\frac{k_f + k_b}{D_B}}}. \quad (\text{F2})$$

This equation only has solutions for $k_f + k_b < D_B/w^2$, which thus gives an upper bound for the reactions rates, above which the homogeneous state is always stable and droplets do not form.

APPENDIX G: STABILITY ANALYSIS OF TERNARY EMULSIONS

The growth rate of droplets in a ternary fluid is given in Eq. (22). There exist stationary states with multiple droplets of equal radii $R_i = \bar{R}$, in which the volume fractions in the background fluid are given by $\phi_0^A = \bar{\phi}_0^A$ and $\phi_0^B = \bar{\phi}_0^B$. The stability of such states can be determined from a linear stability analysis at fixed ϕ_0^A and ϕ_0^B , which yields the perturbation

growth rate

$$\lambda = \frac{D_B \bar{\phi}_0^B}{\psi \bar{R}^2} + \frac{k_s \bar{\phi}_0^A}{\psi} - k_b. \quad (\text{G1})$$

Here $\bar{\phi}_0^A$ can be expressed as

$$\bar{\phi}_0^A \approx \frac{k_b \psi \bar{V} + 4\pi D_B (\gamma\beta - \bar{\phi}_0^B \bar{R})}{k_s \bar{V}} \left[1 - \frac{Q}{k_s \bar{V}} \right], \quad (\text{G2})$$

which follows from Eq. (22) in steady state for weak catalytic cores, $Q \ll k_s \bar{V}$, and $\bar{V} = \frac{4\pi}{3} \bar{R}^3$. Additionally,

$$\bar{\phi}_0^B \approx \phi_+^B(\bar{R}) - \frac{J}{4\pi \bar{R} D_B}, \quad (\text{G3})$$

where J is given by Eq. (11) for $R_i = \bar{R}$ in the case $\bar{R} \ll l$. Inserting these two expressions into Eq. (G1) results in Eq. (24).

-
- [1] M. M. Fryd and T. G. Mason, *Annu. Rev. Phys. Chem.* **63**, 493 (2012).
- [2] C. P. Brangwynne, C. R. Eckmann, D. S. Courson, A. Rybarska, C. Hoegel, J. Gharakhani, F. Jülicher, and A. A. Hyman, *Science* **324**, 1729 (2009).
- [3] C. P. Brangwynne, T. J. Mitchison, and A. A. Hyman, *Proc. Natl. Acad. Sci. USA* **108**, 4334 (2011).
- [4] A. A. Hyman and C. Brangwynne, *Dev. Cell* **21**, 14 (2011).
- [5] D. Zwicker, M. Decker, S. Jaensch, A. A. Hyman, and F. Jülicher, *Proc. Natl. Acad. Sci. USA* **111**, E2636 (2014).
- [6] A. A. Hyman, C. A. Weber, and F. Jülicher, *Annu. Rev. Cell Dev. Biol.* **30**, 39 (2014).
- [7] D. Lingwood and K. Simons, *Science* **327**, 46 (2010).
- [8] P. W. Voorhees, *Annu. Rev. Mater. Sci.* **22**, 197 (1992).
- [9] P. Taylor, *Adv. Colloid Interface Sci.* **75**, 107 (1998).
- [10] B. Dai and L. G. Leal, *Phys. Fluids* **20**, 040802 (2008).
- [11] T. Krebs, K. Schroën, and R. Boom, *Soft Matter* **8**, 10650 (2012).
- [12] E. D. Siggia, *Phys. Rev. A* **20**, 595 (1979).
- [13] M. Feric and C. P. Brangwynne, *Nat. Cell Biol.* **15**, 1253 (2013).
- [14] W. I. Higuchi and J. Misra, *J. Pharm. Sci.* **51**, 459 (1962).
- [15] A. S. Kabalnov, A. V. Pertzov, and E. D. Shchukin, *J. Colloid Interface Sci.* **118**, 590 (1987).
- [16] A. Webster and M. E. Cates, *Langmuir* **14**, 2068 (1998).
- [17] P. Stansell, K. Stratford, J. C. Desplat, R. Adhikari, and M. E. Cates, *Phys. Rev. Lett.* **96**, 085701 (2006).
- [18] K. Stratford, J. C. Desplat, P. Stansell, and M. E. Cates, *Phys. Rev. E* **76**, 030501 (2007).
- [19] G. I. Taylor, *Proc. R. Soc. A* **146**, 501 (1934).
- [20] J. Rallison, *Annu. Rev. Fluid Mech.* **16**, 45 (1984).
- [21] Q. Tran-Cong and A. Harada, *Phys. Rev. Lett.* **76**, 1162 (1996).
- [22] J. J. Christensen, K. Elder, and H. C. Fogedby, *Phys. Rev. E* **54**, R2212 (1996).
- [23] S. C. Glotzer, D. Stauffer, and N. Jan, *Phys. Rev. Lett.* **72**, 4109 (1994).
- [24] S. Toxvaerd, *Phys. Rev. E* **53**, 3710 (1996).
- [25] S. Puri and H. Frisch, *J. Phys. A* **27**, 6027 (1994).
- [26] Q. Tran-Cong, J. Kawai, Y. Nishikawa, and H. Jinnai, *Phys. Rev. E* **60**, R1150 (1999).
- [27] M. Motoyama, *J. Phys. Soc. Jpn.* **65**, 1894 (1996).
- [28] M. Motoyama and T. Ohta, *J. Phys. Soc. Jpn.* **66**, 2715 (1997).
- [29] F. Liu and N. Goldenfeld, *Phys. Rev. A* **39**, 4805 (1989).
- [30] C. B. Muratov, *Phys. Rev. E* **66**, 066108 (2002).
- [31] C. Sagui and R. C. Desai, *Phys. Rev. Lett.* **74**, 1119 (1995).
- [32] R. C. Desai and R. Kapral, *Dynamics of Self-Organized and Self-Assembled Structures* (Cambridge University Press, Cambridge, 2009).
- [33] J. W. Cahn and J. E. Hilliard, *J. Chem. Phys.* **28**, 258 (1958).
- [34] L. Modica, *Arch. Ration. Mech. Anal.* **98**, 123 (1987).
- [35] R. Lefever, D. Carati, and N. Hassani, *Phys. Rev. Lett.* **75**, 1674 (1995).
- [36] D. Carati and R. Lefever, *Phys. Rev. E* **56**, 3127 (1997).
- [37] A. Parmeggiani, F. Jülicher, A. Ajdari, and J. Prost, *Phys. Rev. E* **60**, 2127 (1999).
- [38] T. M. Rogers and R. C. Desai, *Phys. Rev. B* **39**, 11956 (1989).
- [39] I. M. Lifshitz and V. V. Slyozov, *J. Phys. Chem. Solids* **19**, 35 (1961).
- [40] C. P. Brangwynne, *Soft Matter* **7**, 3052 (2011).
- [41] C. A. Ross and M. A. Poirier, *Nat. Med.* **10**, S10 (2004).
- [42] H. Galinski, A. Ambrosio, P. Maddalena, I. Schenker, R. Spolenak, and F. Capasso, *Proc. Natl. Acad. Sci. USA* **111**, 17017 (2014).
- [43] A. Turing, *Phil. Trans. R. Soc. London* **237**, 37 (1952).
- [44] Y. L. Huo, X. L. Jiang, H. D. Zhang, and Y. L. Yang, *J. Chem. Phys.* **118**, 9830 (2003).
- [45] K. Furtado and J. M. Yeomans, *Phys. Rev. E* **73**, 066124 (2006).
- [46] G. R. Dennis, J. J. Hope, and M. T. Johnsson, *Comput. Phys. Commun.* **184**, 201 (2013).